STUDY OF NANOFLUIDS CAVITATING FLOW THROUGH A VENTURI USING COMPUTATIONAL FLUID DYNAMICS CODE

I. BENGHALIA[1,2,a] , N. NEHAOUA[1,b], M. ZAMOUM[2], I. AMI[3,c]

[1] Laboratory of Coatings, Materials, and Environment (LRME), M'Hamed Bougara University of Boumerdes (UMBB), Boumerdes 35000, Algeria
[2] Laboratory of Hydrocarbons Physical Engineering (LGPH), Faculty of Hydrocarbons and Chemistry, M'Hamed Bougara University of Boumerdes, Boumerdes 35000, Algeria
[3] Theoretical Physics and Didactics Laboratory, Faculty of Physics, University of Sciences and Technology Houari Boumediene, Algiers 16000, Algeria
E-mail[a]: l.benghalia@ univ-boumerdes.dz; *E-mail*[b]: n.nehaoua@univ-boumerdes.dz;
E-mail[c]: iami@univ-boumerdes.dz

Received February 13, 2025

Abstract. In this work, we conducted a numerical study of cavitating nanofluid flow through a Venturi. The objective is to investigate the influence of nanoparticles in the base fluid on the cavitation phenomenon. The computational fluid dynamics code (CFD) was selected with a cavitation model. The mixture model for multiphase flow and the k-ω SST turbulence model were adopted. Three fluids were chosen: water, Cu/water and TiO_2/water with different volume franctions of nanoparticle (0%, 10% 20%, 30%) . The simulation was conducted with inlet and outlet pressures set at 700 kPa and atmosphere pressure respectively. The numerical results are compared with the previous experimental and numerical data for flow without nanoparticle. The obtained results found that, the presence of the nanoparticles in the base fluid lead to a slight increase in the static pressure, the position of pressure recovery a significant decrease in fluid velocity and an increase in the vapor fraction formation in the flow. Also, the increase of the nanoparticle volume fractions φ results a decrease in the pressure recovery position, fluid velocity and an increase in the vapor fraction formation. Therefore, the presence of nanoparticles in the base fluid promotes the phenomenon of cavitation.

Key words: hydrodynamic cavitation, Venturi, vapor, CFD, nanofluid.

DOI: https://doi.org/10.59277/RomJPhys.2025.70.609

1. INTRODUCTION

The Cavitation is a liquid vapor phase change phenomenon that appeared in hydraulic systems (pumps, turbines, valves, Venturi tubes, etc.) when the local static pressure drops below the saturated vapor pressure. In liquid flows, this phase change is generally due to local high velocities which induce low pressure. The cavitating flow is a dangerous phenomenon in the field of hydrodynamics, it leads to severe damage problems in hydraulic machinery such as: vibration, bruit and erosion [1]. Many experiments and numerical simulations researchers have investigated to understanding the inception, growth and collapse of cavitation phenomenon through various geometrical [2–4]. Different regimes of cavitation have identified and studied such as including partial cavitation, full developed cavitation and supercavitation [5]. Numerous geometrical parameters of the Venturi have been also studied for better understanding the behavior of cavitation [6–8]. The physical phenomenon involved in the cavitation flow are complex and understanding their mechanisms is essential for industrial safety.

Several researchers have used the Venturi geometry to study the phenomenon of cavitating flow [9–10]. Rudulf *et al.* [5] experimentally analyzed the different cavitation regimes in a convergent-divergent nozzle, including partial cavitation, full developed cavitation and supercavitation. The number of cavitation decreases with the transition between these regimes, from the beginning of cavitation to the supercavitation regime, which is also characterized by a significant increase in vibration and noise. Xu *et al.* [11] made calculations to study two-phase flows through different cavitating Venturis with a homogeneous fluid, using the K-W turbulence model. The influences of pressure, density and current lines on the performance of the Venturi have been discussed. The obtained results showed that the length of the cavity increases as the cavitation number decreases. Barre *et al.* [12] conducted a comparison between numerical (CFD) and experimental methods to analyze sheet cavitation inside a Venturi. They used a dual optical probe to examine void ratio and fluid velocity fields. Also, Lui *et al.* [13] performed numerical simulation work using CFD to investigate the thermodynamic cavitation model in high temperature flows. This study showed that the length of the cavity area decreases with an increase in temperature for the NACA 0015 hydrofoil model. Additionally, for the circular nozzle, they simulated the influence of temperatures (25°C, 50°C, 100°C) on the distribution of vapor.

Abdulaziz [14] conducted experimental investigations for the image of the cavitation process in a small Venturi. He showed that cavitation occurs at a critical pressure ratio of (0.7, 0.72) at $T = 21$°C where the liquid starts to evaporate at the throat of the Venturi.

On the other hand, several researchers have studied nanofluids flows with the aim of enhancing heat transfer. The results obtained show that the presence of nanoparticles in a fluid increases heat transfer [15–17]. Several types of nanofluids have been studied. The results obtained show that the presence of nanoparticles, namely: Al_2O_3/water, TiO_2/water, ZnO/water, and SiO_2/water [18–20].

In this paper, we numerically investigate the nanofluids cavitating flow through a Venturi which the cavitation model was selected and solved using commercial CFD code. The purpose of our work is to study the effect of the presence of nanoparticles in the fluid on the cavitating phenomenon. For this aim, we have selected three different types of fluids, including water, Cu/water and TiO_2/water with various nanoparticle volume fractions of 0%, 10%, 20% and 30%.

2. MODEL EQUATIONS

2.1. A MULTIPHASE AND TURBULENCE MODELS

The equations governing the continuity and momentum for the liquid-vapor mixture model are expressed as:

$$\frac{\partial}{\partial t}(\rho_m) + \nabla \cdot (\rho_m \vec{v}_m) = 0 \tag{1}$$

$$\frac{\partial}{\partial t}(\rho_m \vec{v}_m) + \nabla \cdot (\rho_m \vec{v}_m \vec{v}_m) = -\nabla p + \nabla \cdot [\mu_m (\nabla \vec{v}_m + \nabla \vec{v}_m^T)] + \rho_m \vec{g} + \vec{F} \tag{2}$$

Here ρ_m, $\vec{v}_m$ and μ_m represent the density, velocity and viscosity of the mixture respectively. g is the gravitational acceleration, p is the pressure and $\vec{F}$ is external body force.

The turbulence cavitation flow is characterized by the transport equations for k (turbulent kinetic energy) and ω (specific dissipation rate):

$$\frac{\partial}{\partial t}(\rho k) + \frac{\partial}{\partial x_i}(\rho k u_i) = \frac{\partial}{\partial x_j}\left(\Gamma_k \frac{\partial k}{\partial x_j}\right) + G_k - Y_k + S_k \tag{3}$$

$$\frac{\partial}{\partial t}(\rho \omega) + \frac{\partial}{\partial x_i}(\rho \omega u_i) = \frac{\partial}{\partial x_j}\left(\Gamma_\omega \frac{\partial \omega}{\partial x_j}\right) + G_\omega - Y_\omega + S_\omega \tag{4}$$

2.2. CAVITATION MODEL

Numerous models have been proposed to explore the cavitation process, including those by Dutta *et al.* [28], Singhal *et al.* [21], Schenerr & Sauer [22], and Zwart *et al.* [23]. These models are based on bubble dynamic equation, specifically the Rayleigh-Plesset equation. In our work, the cavitation model developed by Singhal [21] is used. The vapor transport equation can be formulated as:

$$\frac{\partial}{\partial t}(\rho_m f) + \nabla \cdot (\rho_m \vec{v}_m f) = \nabla \cdot (\Gamma \nabla f) + R_e - R_c \tag{5}$$

Here, f signifies the mass fraction, R_e and R_c represent mass transfer source terms connected to the growth (evaporation) and collapse (condensation) of the vapor bubble. The relationship between the mass fraction and density is given by:

$$\frac{1}{\rho_m} = \frac{f}{\rho_v} + \frac{1-f}{\rho_l} \tag{6}$$

where ρ_l and ρ_v are the liquid and vapor densities, respectively. The vapor void fraction is determined by the equation:

$$\alpha = f\frac{\rho_m}{\rho_v} \tag{7}$$

The integration of evaporation and condensation terms with the reduced Rayleigh plesset equation leads to the vapor transport equation:

$$\frac{\partial}{\partial t}(\rho_m f) + \nabla\cdot(\rho_m \vec{v}_m f) = (n4\pi)^{1/3} + (3\alpha)^{2/3}\frac{\rho_v\rho_l}{\rho}\left[\frac{2}{3}\left(\frac{P_B - P}{\rho_l}\right)\right]^{1/2} \tag{8}$$

where P_B is the pressure at the bubbles's surface, P is the bulk liquid pressure, n is bubble number density. The phase change equation can be reformulated in terms as function of bubble radius:

$$R_e = \frac{3\alpha}{R_B}\frac{\rho_v\rho_l}{\rho_m}\left[\frac{2}{3}\left(\frac{P_B - P}{\rho_l}\right)\right]^{1/2} \tag{9}$$

where R_B is the bubble radius calculated by using correlation [18].

$$R_B = \frac{0.061\mathrm{We}\sigma}{2\rho_l v_{rel}^2} \tag{10}$$

with σ – the surface tension, We – the weber number and v_{rel} – the relative velocity defined by $v_{rel}^2 = v_{ch} = \sqrt{k}$, where $\sqrt{k}$ is local turbulence intensity and v_{ch} is the characteristic velocity.

The models for the evaporation and condensation processes are represented as:

If $P < P_v$

$$\mathrm{R_e} = C_1\frac{\max(1.0,\sqrt{k})}{\sigma}\rho_v\rho_l\left[\frac{2}{3}\left(\frac{P_v - P}{\rho_l}\right)\right]^{1/2}\left(1 - f_v - f_g\right) \tag{11}$$

If $P > P_v$

$$R_c = C_2\frac{\max(1.0,\sqrt{k})}{\sigma}\rho_v\rho_l\left[\frac{2}{3}\left(\frac{P - P_v}{\rho_l}\right)\right]^{1/2} f_v \tag{12}$$

where P_v denotes the vapor pressure C_1 and C_2 are 0.02 and 0.01 are constant, 0.02 and 0.01 respectively [18].

2.3. THERMOPHYSICAL PROPERTIES OF NANOFLUIDS

The volume fraction of nanoparticles, denoted as φ represents the ratio of the volume of nanoparticles to the total volume (fluid + solid)

$$\varphi = \frac{V_S}{V_T} \tag{13}$$

where V_S and V_T are the solid volume and the total volume of the nanofluid respectively. The thermophysical properties are calculated by using the following relations:

- The density of nanofluid is calculated by:

$$\rho_{nf} = (1-\varphi)\rho_f + \varphi\rho_p \tag{14}$$

where $\rho_{nf}, \rho_f, \rho_p$ are the densities of nanofluid, base fluid and solid nanoparticles respectively.

- The specific heat capacity is calculated by [24]:

$$(C_P)_{nf} = (1-\varphi)(C_P)_f + \varphi(C_P)_p \tag{15}$$

where $(C_P)_{nf}, (C_P)_f, (C_P)_p$ are the specific heat capacities of nanofluid, base fluid and solid nanoparticles respectively.

- The dynamic viscosity of a nanofluid is calculated by [25]:

$$\mu_{nf} = \frac{\mu_f}{(1-\varphi)^{2.5}} \tag{16}$$

where μ_{nf}, μ_f are dynamic viscosity of nanofluid and the base fluid.

- The thermal conductivity of nanofluid is calculated by [26–27]

$$\frac{\lambda_{nf}}{\lambda_f} = 11.6\varphi^2 + 9.6\,\varphi + 1 \tag{17}$$

where λ_{nf}, λ_f are thermal conductivity of nanofluid and the base fluid.

3. RESULTS AND DISCUSSIONS

3.1. GEOMETRY

The numerical result of cavitating flow was obtained in a Venturi geometry Fig. 1. This Venturi has been used by several researchers [14–28]. The figure presents the schematic of the Venturi with inlet and outlet diameters of Venturi set at 20 mm, the throat diameter of 3.6 mm, the baseline value of the throat is 9 mm, and the convergent and divergent angles are 6.2°.

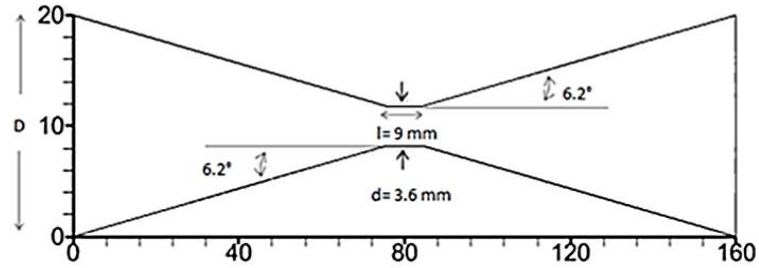

Fig. 1 – Geometry of Venturi.

3.2. MESH INDEPENDENCY

In this section the investigation into the accuracy of numerical simulations involved varying the number of cells (20k, 45k, 60k, 86k, 120k, and 190k) in this research. The influence of mesh size on the static pressure distribution along the axis of the Venturi (Fig. 1) was highlighted under the conditions of 3 bars pressure at the inlet, and atmospheric pressure. Remarkably, it was observed that the results obtained with 86,000, 120,000, and 190,000 cells yielded similar results. Consequently, 86,000 cells were identified as the optimal mesh size for all investigations conducted in this study. Mesh sensitivity is illustrated and compared in Fig. 2.

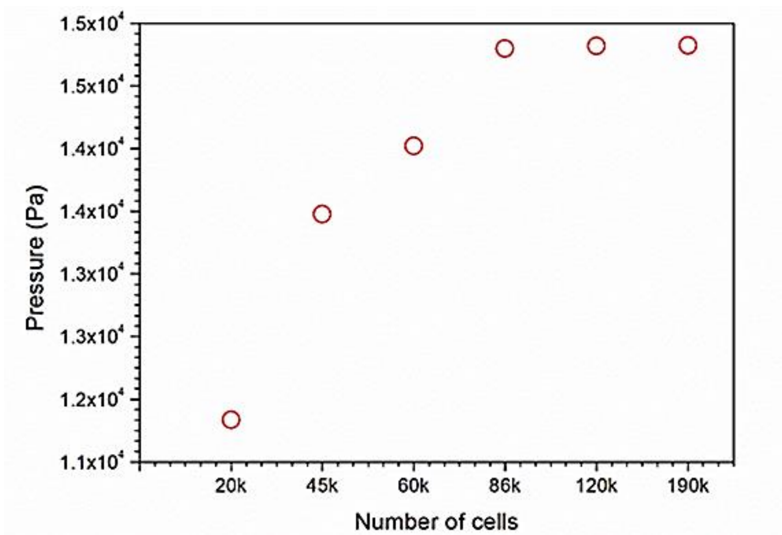

Fig. 2 – Sensitivity analysis of numerical results from computational cells.

The governing equations of the model, as previously detailed, were solved using a CFD code. The KWSST turbulence model was employed to solve the Reynolds-averaged Navier-Stokes (RANS) equations in steady-state conditions. The simulation adopted a mixture multiphase model with a no-slip velocity boundary condition between liquid and vapor phases. A 2D axisymmetric model was utilized with fixed outlet and inlet pressure boundary conditions. For this simulation, the Singhal cavitation model was specifically selected. The pressure-velocity coupling employed a simple algorithm, and the PRESTO discretization scheme was applied for the pressure. A first-order discretization scheme was used for momentum, turbulent kinetic energy, specific dissipation rate, and vapor fraction to ensure and validate the convergence of the simulations.

3.3. VALIDATION

Using the computational fluid dynamics CFD, the numerical resolution of the system equations allowed us to present the effect of the pressure ratios on mass flow rate. To validate our results, we have chosen the experimental data of Abdulaziz [14] and numerical data of Dutta *et al.* [28] (Fig. 3). This figure shows the variation of mass flow rate as function of pressure ratio (P_r) for two fixed inlet pressures 2 and 3 bars. For the inlet pressure 2 bars, our results were compared with the experimental data of Abdulaziz (2014). While for an inlet pressure fixed at 3 bar, our findings were compared also with experimental data of Abdulaziz [14] and numerical data from Dutta *et al.* [28]. The numerical results here were in good agreement with experimental data of Abdulaziz [14], with a difference of 2.38–7.6% for the fixed inlet pressure at 2 and 3 bars, respectively.

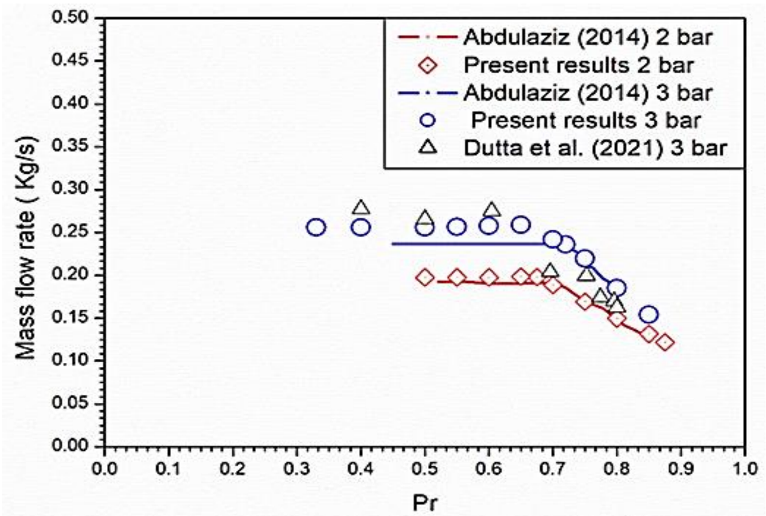

Fig. 3 – Comparison of experimental [14] and numerical [25] results of mass flow rate *versus* pressure ratio.

3.4. EFFECT OF DIFFERENT NANOFLUIDS ON CAVITATION PHENOMENON

In this section, we have chosen three different fluids water, Cu/water and TiO_2/water with the fractions of the nanoparticles in water is 10% for study the effects of nanofluids on cavitation phenomenon formation. The inlet and outlet pressures of the Venturi are 700 kPa and atmosphere pressure, respectively. Subsequently, the pressure, the velocity distributions and the fraction vapor formation are provided in detail. The physical properties of the liquid and nanofluids used in this study are presented in the Table 1.

Table 1

Physical properties of the liquid and nanoparticles used

	Density (kg/m^3)	Thermal Conductivity (W/ m·K)	Specific heat (J/kg·K)	Viscosity (Pa·s)
Water	997.1	0.613	4179	0.00096
Cu	8933	400	385	–
TiO_2	4250	8.95	686.2	–
Cu/water	1790.69	1.2725	3799.6	0.00124
TiO_2/water	1322.39	1.2725	3829.72	0.00124

Figure 4 illustrates the distribution of static pressure across a Venturi for different nanofluids water, Cu/water, TiO_2/water. For all fluids, it can be observed that the static pressure gradually decreases in the convergent section of the Venturi. In the throat section, the static pressure continues to decrease until it reaches the minimum pressure (minimum vapor pressure) and remains constant through the divergent section. In this divergent section, the pressure of each nanofluid begins to increase "pressure recovery" at different positions for water, water/ TiO_2, water/Cu, respectively. This position of pressure recovery changes slightly with the type of the nanofluid. This difference is due to the physical properties of the nanofluids.

The evolution of fluid velocity along the axis of the Venturi is shown in the Fig. 5. It can be observed that the fluid velocity varies inversely with pressure (according to Bernoulli's low). In the convergent part of the Venturi, the velocity of the water is better than the velocity of TiO_2/water and Cu/water respectively. At the throat of the Venturi, the velocity of the water and nanofluids reaches its maximum value. Notably, this maximum value of fluid velocity strongly depends on the nature of the fluid. Moreover, the maximum velocities at the throat are: 37.49 m/s, 32.61 m/s and 28.09 m/s for water, TiO_2/water, Cu/water respectively. This variation is due to viscosity of nanofluid. Indeed, the presence of the nanoparticles in the fluid increases its viscosity, which consequently decreases the fluid velocity.

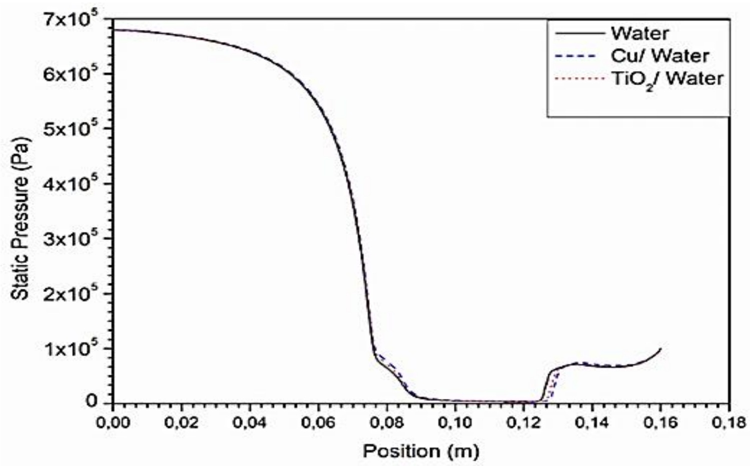

Fig. 4 – Pressure distribution along the Venturi tube for water, Cu/water and/ TiO2/water with φ = 10%.

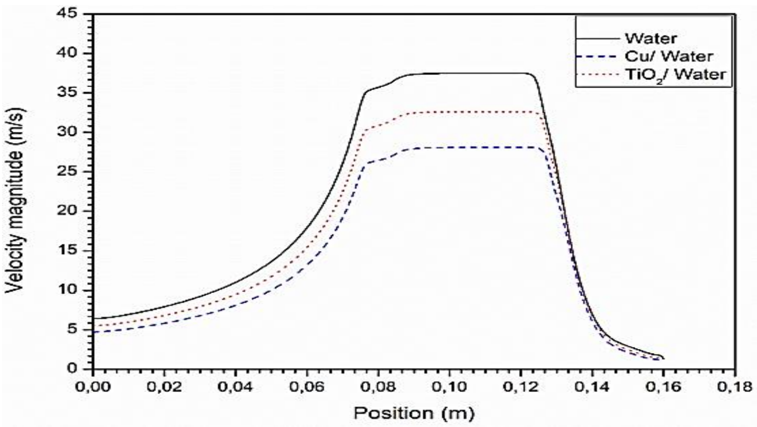

Fig. 5 – Velocity magnitude *versus* axial length of the Venturi for water, Cu/water and TiO_2/water with φ = 10%.

Figure 6 shows the distribution of vapor formation for the water and nanofluids Cu/water and TiO_2/water through the Venturi. It can be observed that the vapor fraction formation is better for the nanofluids Cu/Water compared to the TiO_2/ water and Water, the existence of the nanoparticle favors the formation of vapor bubbles and by consequently cavitation phenomenon. The vapor formation increases progressively until it reaches the maximum value 0.568, 0.6 and 0.64 for water, TiO_2/water and Cu/water respectively. Additionally, for all fluids, the vapor formation is located and concentrated in the divergent part of Venturi which starting at the end of the throat (the beginning of the divergent part) (Fig. 7). Therefore, the existence of nanoparticles in water leads to an increase on the intensity of cavitation phenomenon.

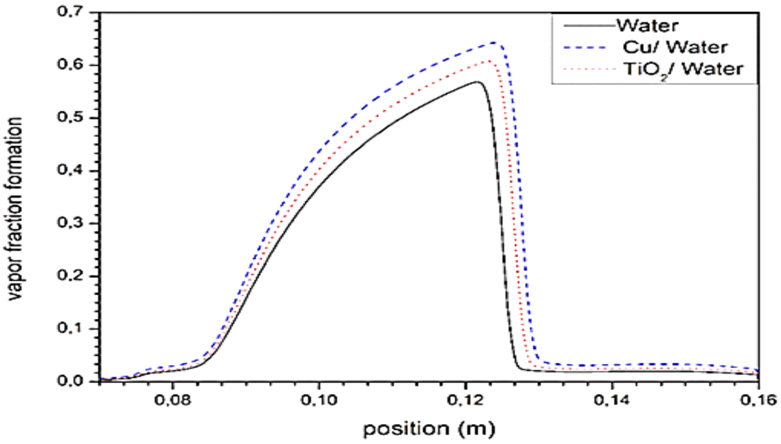

Fig. 6 – Vapor volume fraction along the Venturi for water, Cu/water and/ TiO_2/water with φ = 10%.

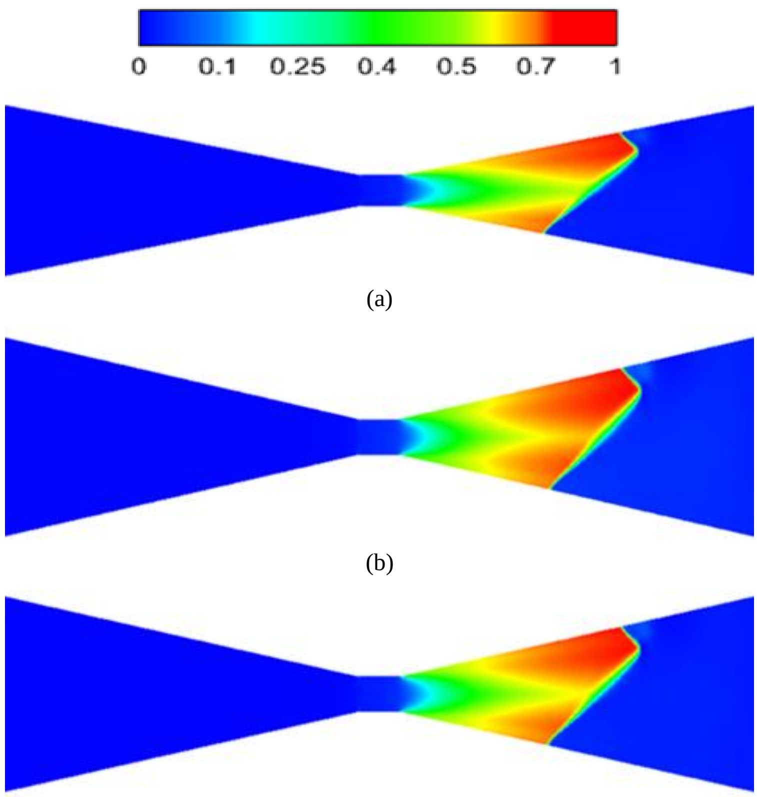

(a)

(b)

(c)

Fig. 7 – Contours of vapor volume fraction along the Venturi for:
a) water; b) Cu/water; c) TiO_2/water with φ = 10%.

3.5. INFLUENCE OF THE FRACTIONS OF NANOPARTICLE IN THE BASE FLUID ON THE CAVITATION PHENOMENON

For study the effect of nanoparticle fraction φ in cavitation phenomenon, we have chosen four fractions of Cu nanoparticles in water: 0%, 10%, 20%, and 30%. The inlet and outlet pressures are 700 kPa and atmosphere pressure, respectively. Subsequently, pressure distribution, fluid velocity and fraction vapor formation are provided in detail.

Figure 8 shows the distribution of static pressure across a Venturi for different fractions φ of nanoparticle Cu 0%, 10%, 20%, 30%. For all various fractions of nanoparticles, it can be observed that the static pressure similarly decreases in the convergent section of the Venturi. At the throat section, the static pressure continues to decrease with slight difference until it reaches the minimum pressure and remains constant. In divergent section, the pressures of different fractions of nanoparticles begin to an increase at specific positions. Indeed, the pressure recovery decreases insignificantly with increasing nanoparticle fractions.

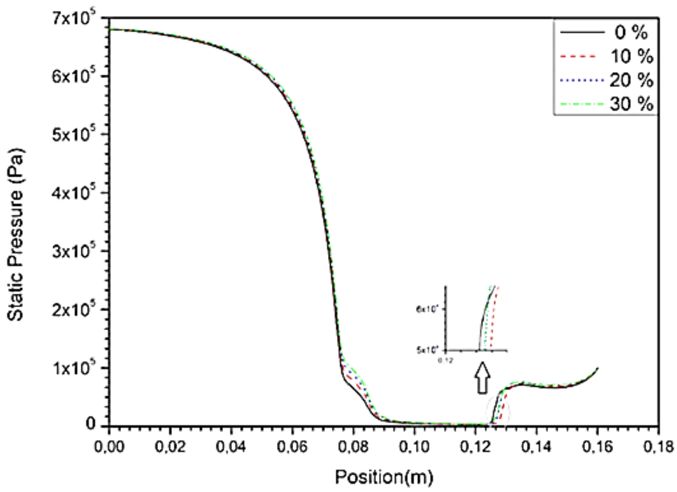

Fig. 8 – Pressure distribution along the Venturi tube for different nanoparticle fractions of Cu 0%, 10%, 20%, and 30%.

Figure 9 shows the evolution of fluid velocity along the axis of the Venturi for various fractions of nanoparticle φ in the water. The curves in this figure have the same profile regardless the fractions of nanoparticle Cu. Also, we noted that the fluid velocity is higher for the fluid without nanoparticles. Increasing the nanoparticle fraction leads to a decrease in the fluid velocity. Indeed, the maximum value of fluid velocity at throat are: 37.49 m/s, 28.09 m/s, 23.47 m/s, and 20.59 m/s for 0%, 10%, 20%, 30% respectively. The increase in the volume fraction of the particles leads to the increase in the viscosity of the nanofluid and consequently the decrease in the flow velocity.

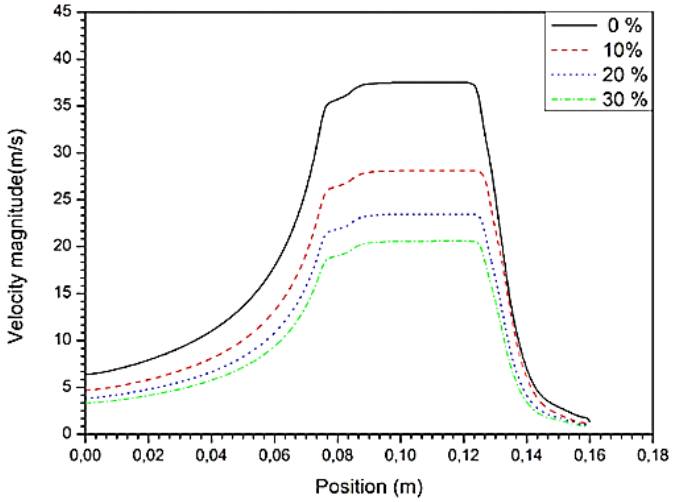

Fig. 9 – Velocity magnitude *versus* axial length of the Venturi for different nanoparticle fractions of Cu 0%, 10%, 20%, and 30%.

Figure 10 illustrates the distribution of vapor formation for the different fractions of nanoparticle Cu 0%, 10%, 20% and 30% through the Venturi. It can be noted that the vapor formation gradually rises until it reaches its maximum values of 0.568 for 0%, 0.64 for 10%, 0.67 for 20% and 0.685 for 30%. Additionally, the vapor fraction formation increases with increasing fraction of nanoparticles until 20%. Beyond, this value the effect of nanoparticles on the base fluid decreases. Therefore, the vapor formation is strongly influenced by lower value of the nanoparticle fractions. However, at higher nanoparticle fractions, the effect on cavitation decreases.

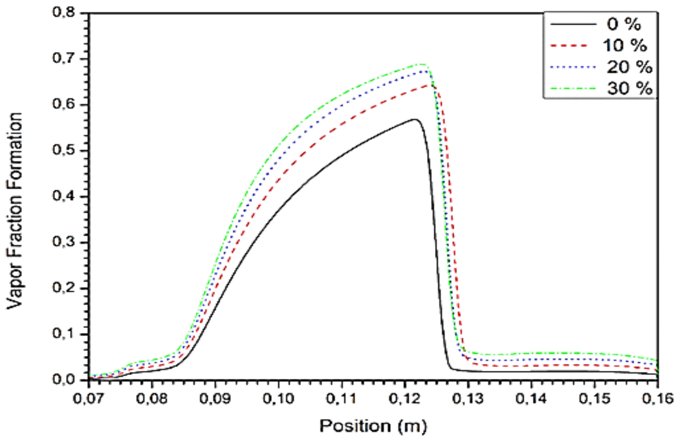

Fig. 10 – Vapor distribution through a Venturi for different nanoparticle fractions of Cu: a) 0%; b) 10%; c) 20%; d) 30%.

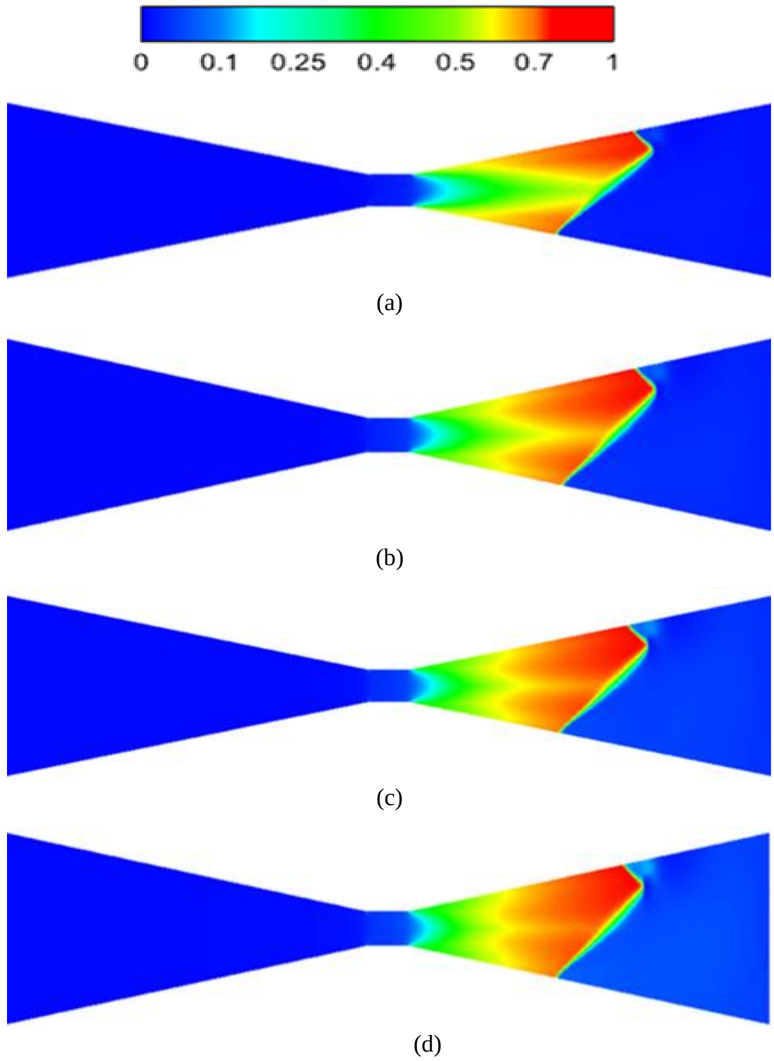

Fig. 11 – Contours of vapor fraction formation through a Venturi for different nanoparticle fractions of Cu: a) 0%; b) 10%; c) 30%; d) 40%.

4. CONCLUSION

In this work, we conducted a numerical study using computational fluid dynamics code (CFD) to investigate the effect of nanofluids cavitating flow phenomenon through a Venturi nozzel. The mixture model for multiphase flow and the k-ω SST turbulence model were adopted. Three different fluids were chosen; water, Cu/water and TiO_2/water with various nanofluid volume franction of 0%, 10%, 20% and 30%.

The simulation was conducted with inlet and outlet pressures set at 700 kPa and atmosphere pressure respectively.

The obtained results found that the existence of the nanoparticles in the base fluid lead to:

✓ A slight increase in the fluid static pressure and also increase position of pressure recovery.

✓ An important decrease in the fluid velocity.

✓ An increase in the vapor fraction formation in the flow.

Also, the obtained results found that the effect of the volume fractions φ of the nanoparticles on the cavitating flow. The increase of the volume fractions lead to:

✓ The slight decrease in pressure recovery.

✓ The fluid velocity decreases significantly.

✓ The increase in vapor fraction formation.

Therefore, the presence of the nanoparticles in the base fluid promotes vapor production and consequently, enhances the cavitation phenomenon. Indeed, the nanoparticles act as nucleation sites, facilitating the formation of the vapor phase.

Nomenclature				
d	throat Diameter of Venturi		V_m	mixture volume phase
D	diameter of Venturi		We	Weber number
Cp	specific heat capacity		x_i	cartesian coordinate along position index i
f	mass fraction		x_j	cartesian coordinate along position index j
$\vec{F}$	external force body		Y_k	dissipation of the turbulent kinetic energy
$\vec{g}$	gravitational acceleration		Y_w	dissipation of the specific dissipation rate
G_k	generation of turbulent kinetic energy			
G_ω	generation of the specific dissipation rate		α	vapor void fraction
l	throat length of the Venturi		μ	dynamic viscosity
n_b	bubble number density		ρ	density
P	pressure of liquid		σ	surface tension
P_B	bubble pressure		φ	volume fraction of nanoparticles
P_v	vapor pressure saturation		λ	the thermal conductivity
R	radius			
R_B	bubble radius		c	condensation
R_c	mass transfer of condensation		e	evaporation
R_e	mass transfer of evaporation		f	base fluid
S_k	source terms of the turbulent kinetic energy		g	non-condensable gas
S_W	source of the specific dissipation rate		l	liquid
v	velocity		m	mixture
v_{ch}	characteristic velocity		nf	nanofluids
v_m	the mass-averaged velocity		P	solid nanoparticles
v_{rel}	relative velocity		th	throat
V_v	vapor, volume phase		v	vapor

REFERENCES

1. J. P. Franc and J. M. Michel, *Fundamentals of cavitation*, Springer science & Business media, 2006.
2. B. Ebrahimi *et al.*, International Journal of Thermal Sciences **114**, 229–240 (2017).
3. N. T. Thang, D. Ngoc, Fluid Dyn. **54**, 835–849 (2019).
4. J. Cai, X. Huai and X. Li, J. Therm. Sci. **18**, 338–344 (2009).
5. P. Rudolf, M. Hudec, M. Gríger, D. Stefan, EPJ Web Conf. **67**, 02101, 25 Marzo (2014).
6. H. Ghassemi and H.F. Fasih, Flow Measurement and Instrumentation **22**, 406–412 (2011).
7. A. Simpson and V. V. Ranade, Chemical Engineering Research and Design **136**, 698–711(2018).
8. T. A. Bashir *et al.*, The Canadian Journal of Chemical Engineering **89**(6), 1366–1375 (2011).
9. M. Zamoum and M. Kessal, Scientific Research and Essays **10**(11), 367–375 (2015).
10. B. Rostane *et al.*, Thermal Science **27**(4B), 3467–3475 (2023).
11. C. Xu, S. D. Heister and R. Field, Journal of Propulsion and Power **18**(6), 1227–1234 (2002).
12. S. Barre *et al.*, European Journal of Mechanics – B/Fluids **28**(3), 444–464 (2009).
13. D. M. Liu *et al.*, Thermal Science **15**(suppl. 1), 95–101(2011).
14. A. M. Abdulaziz, Experimental Thermal and Fluid Science **53**, 40–48 (2014).
15. R. Djebali, Romanian Journal of Physics **65**, 122 (2020).
16. C. V. Vraciu, R. Iovanescu, Romanian Journal of Physics **66**, 111 (2021).
17. M. Ferhi and R. Djebali, Romanian Journal of Physics **67**, 605 (2022).
18. P. Barnoon, D. Toghraie, F. Eslami, and B. Mehmandoust, Comput. Math. Appl. **77**, 662–692 (2019).
19. A. Rezaei Gorjaei, M. Soltani, M. Bahiraei and F. M. Kashkooli, Int. J. Mech. Sci. **146–147**, 396–404 (2018).
20. M. Sivashi and M. Janali, J. Cent. South Univ. **24**, 1850–1865 (2017).
21. A.K. Singhal, M.M. Athavale, H. Li and Y. Jiang, Journal of Fluids Engineering **124** (3), 617–624. (2002).
22. G. Schnerr and J. Sauer, *Physical and numerical modeling of unsteady cavitation dynamics*, Proceeding of 4th International Conference on Multiphase Flow, 1–12, New Orleans, USA, 2001. https://www.researchgate.net/publication/29619675
23. P.J. Zwart, A.G. Gerber and T. Belamri, *A two-phase flow model for predicting cavitation dynamics*, Journal Fifth International Conference on Multiphase Flow, Yokohama, Japan, 2014.
24. B.C. Pak and Y.I. Cho, Experimental Heat Transfer **11**(2), 151–170 (1998).
25. H.C. Brinkman, J. Chem. Phys. **20**, 571–581 (1952).
26. C. Maxwell, *A Treatise on electricity and magnetism*, Clarendon Press, U.K., 1891.
27. R.L. Hamilton and O.K. Crosser, Industrial and Engineering Chemistry Fundamentals **1**(3), 187–191 (1962).
28. N. Dutta, P. Kopparthi, A.K. Mukherjee, N. Nirmalkar and G. Boczkaj, Water Res. **204**, 117559 (2021).